# Dynamics of a passive micro-vibration isolator based on a pretensioned plane cable net structure and fluid damper

**Yanhao Chen, Qi Lu, Bo Jing and Zhiyi Zhang**

Institute of Vibration, Shock and Noise, Shanghai Jiao Tong University, Dongchuan Road 800, 200240, Shanghai, China

E-mail: chychang@sjtu.edu.cn, chen_hao@sjtu.edu.cn

**Abstract.** This paper addresses dynamic modelling and experiments on a passive vibration isolator for application in the space environment. The isolator is composed of a pretensioned plane cable net structure and a fluid damper in parallel. Firstly, the frequency response function (FRF) of a single cable is analysed according to the string theory, and the FRF synthesis method is adopted to establish a dynamic model of the plane cable net structure. Secondly, the equivalent damping coefficient of the fluid damper is analysed. Thirdly, experiments are carried out to compare the plane cable net structure, the fluid damper and the vibration isolator formed by the net and the damper, respectively. It is shown that the plane cable net structure can achieve substantial vibration attenuation but has a great amplification at its resonance frequency due to the light damping of cables. The damping effect of fluid damper is acceptable without taking the poor carrying capacity into consideration. Compared to the plane cable net structure and the fluid damper, the isolator has an acceptable resonance amplification as well as vibration attenuation.

## 1. Introduction

The term micro-vibration usually refers to low-level mechanical vibration or disturbance in the microgravity environment, typically occurring at frequency from less than 1 Hz up to 1 kHz[1]. Therefore, micro-vibration can be generated by mechanical system on board space crafts, such as reaction/ momentum wheel assemblies (R/MWAs), cryo-coolers, thrusters, solar array drive mechanisms and mobile mirrors, etc. Due to very tiny environmental damping in aerospace, micro-vibration could persist for a long time. Obviously, vibration has long been serious problems to cause damage to the payloads or degrade its performance, which may be happened on-orbit.

To meet the requirement of more strict vibration targets, both passive and active isolation solutions, damping enhancing measures as well as structures with inherent vibration isolation properties have been proposed [2-5]. The main disturbance source of on-orbit spacecraft is often mechanical spinning devices such as reaction and momentum wheel assemblies. Wheel assemblies are widely used in space technology to provide attitude control and momentum stability of a spacecraft. Many passive and active vibration isolation systems have been designed and researched to attenuate the vibrations on space crafts. Honeywell [6] developed a viscous-damped passive isolator for the Hubble Space Telescope to suppress the vibrations from RWAs. Vaillon and Philippe [7] designed and tested an elastomer-based passive vibration isolator. The isolator can be used to isolate the six degrees of freedom of a disturbance source with an attenuation performance exceeding 20dB above 25Hz and 40dB above 50Hz. Makiharaetal [8] studied a semi-active vibration isolator for momentum wheel assemblies, which is stable even when a control malfunction occurs. Kameshaetal [2] proposed a flexible low-frequency platform for RWAs

consisting of four folded beams, and the finite element method(FEM)was used to analyse its passive and active vibration isolation performance. Typical isolation systems for space optical telescopes, referred to as vibration isolation and suppression system and satellite ultra-quiet isolation technology experiment having been developed and utilized in spacecraft, can be seen in [9, 10] . The VISS and SUITE consisting of six struts in a hexapod configuration are used as the support of the sensitive payloads or the disturbance sources of on board spacecraft. Many other isolation systems are designed as support structures of payloads, which can isolate the micro-vibration transmitted from disturbance of the spacecraft to the sensitive payloads. The suppression of micro-vibration in the propagation path of disturbances has also been studied.

For spacecraft applications, one most important factor that should be considered is the lightweight and cost effective. Also should bear in mind is the inherent on-orbit micro-vibration properties, which may hamper some measures of which the performance depends on the vibration amplitude of the host structure, such as dynamic vibration absorber as well as viscoelastic damping layers. As suggested in [11], dry friction is not desired in spacecraft applications thanks to the micro-amplitude vibration. On the other hand, the on-orbit vibration of space systems can be considered as linear vibration by neglecting the fretting wear and micro slip along the interfaces.

In this paper, the coupled function between transversal vibration and longitudinal vibration is analysed. The tension variation caused by transversal vibration and longitudinal vibration is computed. The mechanical mobility method is developed to model the pretensioned plane cable net structure, which is composed of 8 cables. The performance of the proposed plane cable net structure is dependent only on the pretension force, making it a candidate for spacecraft micro-vibration isolation. Taking the small vibration amplitude of the cables into consideration, a fluid damper is designed and analysed. Besides, the force transmissibility of the plane cable net structure is tested. Experiments on the plane cable net structure, the fluid damper and the isolation device made up by the former two were carried out, respectively. Result shows that the plane cable net structure can achieve substantial vibration attenuation, with the resonance peak having a great amplification due to the lower damping coefficient of cables. While the damping effect of the fluid damper is acceptable without taking the poor carrying capacity into consideration. Compared to the plane cable net structure and the fluid damper, the isolator has an acceptable resonance amplification and vibration attenuation rate.

## 2. Tension variation in string caused by vibrations

A real string is vibrating in two transversal planes, and in the longitudinal direction as well. For simplicity, assuming that the string is vibrating in one plane, thus, one transversal and one longitudinal vibration is present. When a transversal displacement occurs on the string, the string elongates. This results in a force exciting a longitudinal wave in the string [12]. The longitudinal wave modulates the tension of the string, which influences the transversal vibration. Note that throughout this section losses and dispersion are not considered, since now coupling between the two polarizations is what concerned.

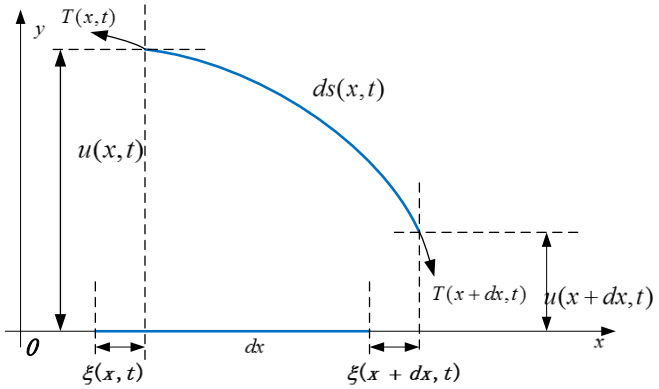


**Figure 1.** The string element model.

The element of length $dx$ at equilibrium will have the length $ds$ after vibrating. where $u = u(x,t)$ and $\xi = \xi(x,t)$ are the transversal and longitudinal displacements of the string with respect to time $t$ and space $x$, as depicted in figure 1. The initial tension of the string is $T_0$. the Deformation equation is

$$(ds)^2 \approx \left[\xi(x+dx,t)-\xi(x,t)+dx\right]^2 + \left[u(x+dx,t)-u(x,t)\right]^2 \tag{1}$$

As $dx$ is infinitesimally small, the differences are substituted by differentials:

$$ds = \sqrt{\left(\frac{\partial \xi}{\partial x}+1\right)^2 \cdot (dx)^2 + \left(\frac{\partial u}{\partial x}\right)^2 \cdot (dx)^2} = \sqrt{\left(\frac{\partial \xi}{\partial x}+1\right)^2 + \left(\frac{\partial u}{\partial x}\right)^2}\, dx \tag{2}$$

As the length of the element changes varies the tension $T = T(x,t)$ of the string according to the Hooke's law:

$$T = T_0 + EA\left(\frac{ds}{dx}-1\right) \tag{3}$$

where $E$ is the Young's modulus and $A$ is the cross-section area of the string. By substituting equation (2) into equation (3), the string tension can be approximated as:

$$T \approx T_0 + EA\left[\frac{\partial \xi}{\partial x}+\frac{1}{2}\left(\frac{\partial u}{\partial x}\right)^2\right] \tag{4}$$

Due to the micro-vibration environment, the segment $ds$ is nearly parallel to the $x$ axis, and the longitudinal force on the segment $ds$ is the difference of the tension at the sides of the segment:

$$F_l \approx \frac{\partial T}{\partial x}dx \approx EA\left(\frac{\partial^2 \xi}{\partial x^2}+\frac{1}{2}\cdot\frac{\partial\left(\partial u/\partial x\right)^2}{\partial x}\right)dx \tag{5}$$

This force acts on a mass $\mu dx$, where $\mu$ is the mass per unit length. Accordingly, the longitudinal vibration is approximately described by the following equation:

$$\mu\frac{\partial^2 \xi}{\partial t^2} = EA\frac{\partial^2 \xi}{\partial x^2}+\frac{1}{2}EA\frac{\partial\left(\partial u/\partial x\right)^2}{\partial x} \tag{6}$$

The above formula shows that the string longitudinal displacement varies with transversal motion during vibration. The longitudinal vibration can also result in the string tension variation, which finally will act on the transversal string motion. The coupling of transversal and longitudinal string motion depends on the magnitude of vibration according to a square law.

According to equation (4), influence of the string's longitudinal and transversal vibration on the string tension variation can be written as

$$\Delta T = T - T_0 = EA\frac{\partial \xi}{\partial x}+\frac{1}{2}EA\left(\frac{\partial u}{\partial x}\right)^2 \tag{7}$$

A single string with both ends fixed, shown in figure 2, is now applied to study the tension variation caused by the transversal and longitudinal vibrations. According to the classical string vibration theory, when excited at $h$, the transversal displacement response of $x$ is described by:

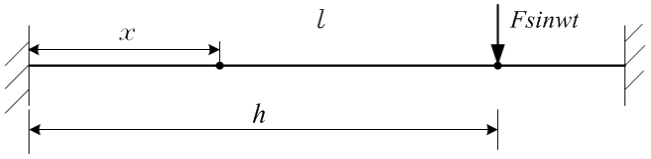


**Figure 2.** Fixed-fixed string with a lateral harmonic force.

$$u(x,t)=\frac{\sin\lambda x\cdot\sin\lambda(l-h)}{T_0\lambda\sin\lambda l}F\sin\omega t \qquad (0\le x\le h) \tag{8}$$

where $\lambda=\omega\cdot\sqrt{\frac{\rho A}{T_0}}$ and $\rho$ is the density of the string.

Simplified from equation (6) , the longitudinal vibration equation can be rewritten in the form:

$$\frac{\partial^2\xi}{\partial t^2}=\frac{E}{\rho}\cdot\frac{\partial^2\xi}{\partial x^2}+\frac{E}{2\rho}\cdot\frac{\partial\left(\partial u/\partial x\right)^2}{\partial x} \tag{9}$$

The differential equation of transversal vibration determined from equation (8) is written as:

$$\frac{\partial\left(\partial u/\partial x\right)^2}{\partial x}=-\lambda\cdot\left(\frac{F\cdot\sin\lambda(l-h)}{T_0\sin\lambda l}\right)^2\cdot\sin 2\lambda x\cdot\sin^2\omega t \tag{10}$$

Supposing that $a^2=\frac{E}{\rho}$, $c=-\lambda\cdot\left(\frac{F\cdot\sin\lambda(l-h)}{T_0\sin\lambda l}\right)^2$, the equation (9) can be simplified as:

$$\frac{\partial^2\xi}{\partial t^2}-a^2\frac{\partial^2\xi}{\partial x^2}=c\cdot\sin 2\lambda x\cdot\sin^2\omega t \tag{11}$$

The boundary conditions are

$$\xi(x,0)=\xi_t(x,0)=0$$

$$u(0,t)=u(l,t)=0$$

With an assumption that $f(x,t)=c\cdot\sin 2\lambda x\cdot\sin^2\omega t$ , $\left(0<x<l,t>0\right)$ ,the longitudinal displacement response function is calculated from equation (11) and takes the form:

$$\xi(x,t)=\sum_{n=1}^{\infty}\left[\int_0^t f_n(\tau)\cdot\sin\frac{n\pi a}{3}(t-\tau)d\tau\right]\cdot\sin\frac{n\pi}{3}x \tag{12}$$

where $f_n(\tau)=\frac{2}{n\pi a}\int_0^l f(x,\tau)\sin\frac{n\pi}{l}xdx$.

After simplification, the longitudinal vibration response function reduces to:

$$\xi(x,t)=\sum_{n=1}^{\infty}p_n\cdot\sin\frac{n\pi}{3}x\cdot\left[\frac{3}{2n\pi a}+(q_n-\frac{3}{2n\pi a})\cdot\cos\frac{n\pi a}{3}t-q_n\cdot\cos 2\omega t\right] \tag{13}$$

where

$$p_n=\frac{c}{n\pi a}\left(\frac{\sin(6\lambda-n\pi)}{2\lambda-\frac{n\pi}{3}}-\frac{\sin(6\lambda+n\pi)}{2\lambda+\frac{n\pi}{3}}\right),\quad q_n=\frac{1}{2}\left(\frac{1}{\frac{2}{3}n\pi a-4\omega}+\frac{1}{\frac{2}{3}n\pi a+4\omega}\right) \tag{14}$$

Equation (8) and equation (13) are the transversal and longitudinal displacements of a string with both ends fixed when excited at $h$, with respect to time $t$ and space $x$. More attention should be paid to the tension variation. From equation (7), the tension variation caused by transversal vibration is expressed as:

$$\left|\Delta P_h\right|=\frac{1}{2}EA\left|\frac{\partial u}{\partial x}\right|^2 \tag{15}$$

From equation (8), the partial differential equation of transversal vibration displacement has the following form:

$$\left|\frac{\partial u}{\partial x}\right| = \left|\frac{\sin\lambda(l-h)}{T_0 \sin\lambda l}\cos\lambda x \cdot F\right| \tag{16}$$

Substituting equation (16) into equation (15), the tension variation caused by transversal vibration with respect to space $x$ can be written as:

$$\left|\Delta P_h\right| = \frac{1}{2}EA\left(\frac{F\sin\lambda(l-h)}{T_0\sin\lambda l}\right)^2 \cos^2\lambda x \tag{17}$$

Specially, at the ends fixed $(x=0)$ , the tension variation is

$$\left|\Delta P_h\right\|_{x=0} = \frac{1}{2}EA\left(\frac{F\sin\lambda\left(l-h\right)}{T_0\sin\lambda l}\right)^2 \tag{18}$$

Accordingly, the tension variation caused by longitudinal vibration can be obtained from equation (7) ,

$$\Delta P_z = EA\frac{\partial\xi}{\partial x} \tag{19}$$

The partial differential equation of longitudinal vibration displacement derived from equation (13) is written as:

$$\frac{\partial\xi}{\partial x} = \sum_{n=1}^{\infty}\frac{3p_n}{n\pi}\cdot cos\frac{n\pi}{3}x\cdot\left[\frac{3}{2n\pi a}+(q_n-\frac{3}{2n\pi a})\cdot\cos\frac{n\pi a}{3}t-q_n\cdot\cos 2\omega t\right] \tag{20}$$

Substituting equation (20) into equation (19) yields the tension variation function caused by longitudinal vibration with respect to space $x$:

$$\Delta P_z = \sum_{n=1}^{\infty}\frac{3EAp_n}{n\pi}\cdot\cos\frac{n\pi}{3}x\cdot\left[\frac{3}{2n\pi a}+(q_n-\frac{3}{2n\pi a})\cdot\cos\frac{n\pi a}{3}t-q_n\cdot\cos 2\omega t\right] \tag{21}$$

Setting that

$$\Psi_1 = \frac{3EAp_n}{n\pi}\cdot\cos\frac{n\pi}{3}x\cdot\frac{3}{2n\pi a} \tag{22}$$

$$\Psi_2 = \frac{3EAp_n}{n\pi}\cdot q_n\cdot\cos\frac{n\pi}{3}x \tag{23}$$

$$\Psi_3 = \frac{3EAp_n}{n\pi}\cdot(q_n-\frac{3}{2n\pi a})\cdot\cos\frac{n\pi}{3}x \tag{24}$$

the equation (21) can be simplified as

$$\Delta P_z = \sum_{n=1}^{\infty}\Psi_1+\sum_{n=1}^{\infty}\Psi_3\cdot\cos\frac{n\pi a}{3}t-\sum_{n=1}^{\infty}\Psi_2\cdot\cos 2\omega t \tag{25}$$

Equation (25) is the tension variation caused by longitudinal vibration displacement, with respect to time $t$ and space $x$. The first two items on the right side of equation (25) denote the transient vibration or free vibration, which is caused by initial conditions and will be decayed soon in case of damping. So in the following part, the effects of the first two items are ignored. The third item is the steady vibration response under external load, which is also the focus of attention.

A both ends fixed string has the following properties: string length $l=0.3m$ ,string cross-section area $A=\pi\times\left(0.0015\right)^2 m^2$, Young's modulus $E=1.4\times10^{11}Pa$, the pretension $T_0=100N$ . A unit harmonic force is applied at the middle of the string, $h=0.15m$ . The magnitude of tension variation, $\left|\Delta P_h\right\|_{x=0}$ and $\Psi_2\big|_{x=0}$, are shown in figure (3).

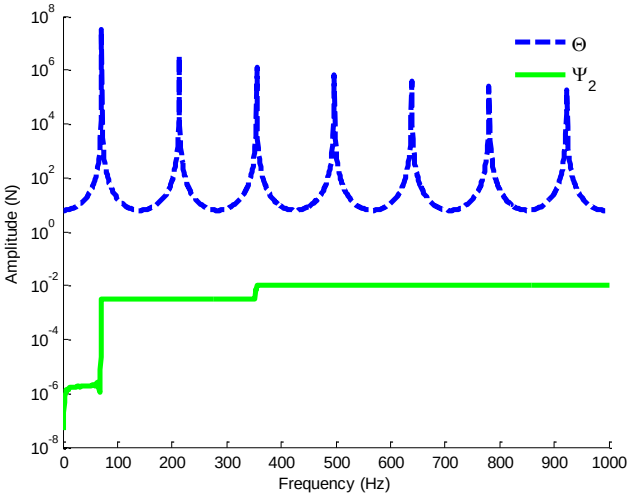


**Figure 3.** The amplitude of the tension variation caused by transversal and longitudinal vibration.

Compared to the tension variation caused by transversal vibration, the amplitude of the $\Psi_2$ is much less. This can be verified the classical string theory, in which the longitudinal vibration of string is ignored.

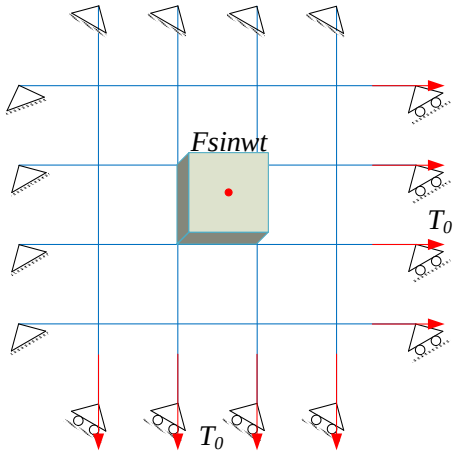


**Figure 4.** The pretensioned plane cable net structure composed of 8 strings.

The plane cable net structure is composed of a plurality of strings with a preload, as shown in figure 4. And the payload is applied to the four intersection chords in the centre of the plane cable net structure. Then the vibration can be transmitted to the fixed points by tension variation of the strings. In this process, the vibration energy is absorbed and released by the string periodically. The mechanical admittance method proposed by Jetmundsen [13] is adopted in the modelling. The string vibration response equations are used to set up the plane cable net structure frequency response functions (FRF). Finally, after coupled with the mass, the FRF of the whole system can be obtained.

Based on the dynamics of single string, a plane cable net model consisting of 8 strings is established. The vibration and force transmissibility of the plane cable net model are analysed. The string length $l = 0.3m$,string cross-section area $A = \pi \times (0.0015)^2\ m^2$, Young's modulus $E = 1.4 \times 10^{11} Pa$. A unit

excitation force is applied at the middle of the mass. The response curves under different pretensions are shown in figure 5. The greater the preload, the greater the first order natural frequency of the string. The load-bearing stiffness of the plane cable net structure will increase with the pretension of the string. Still, the displacement response shown in figure 5(a) is similar to the frequency response characteristics of spring-mass system. Although the dynamics of a single string is very complicated, the direct response of the mass in the centre of the cable net is much easier to understand.

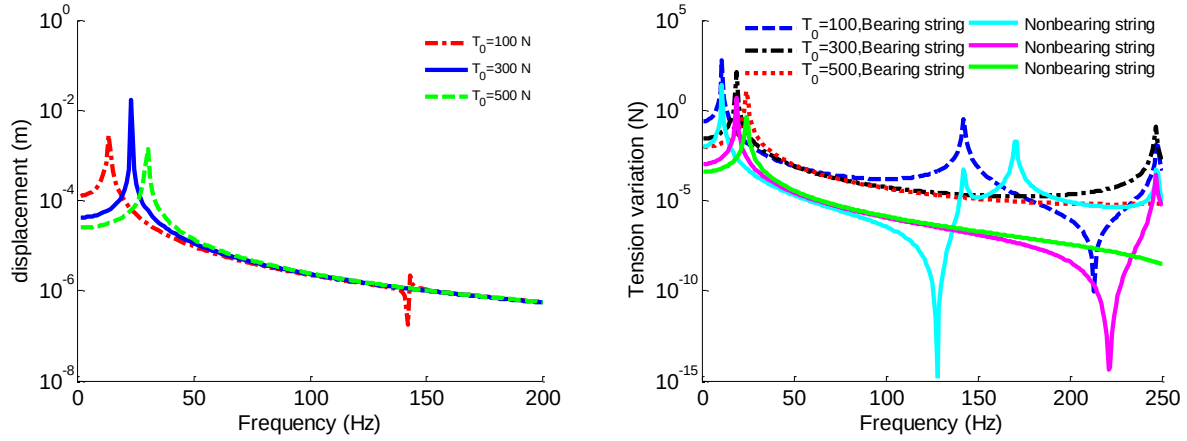


**Figure 5.** (a) is the direct displacement frequency response of the mass and (b) is the tension variation at the fixed ends of the bearing string and non-bearing string.

## 3. The fluid damper

In the micro-vibration situation, the vibration amplitude is small. And the relative displacement among strings is small, which results in that just a little vibration energy can be dissipated by friction. In order to achieve a better vibration attenuation, it's essential to add a damping device in the plane cable net structure. As shown in figure 6 (a), the fluid damper is made up by two bellows. When an external force is applied to the upper surface of the fluid damper, the lower bellows will shrink, which leads to the fluid flowing upward. The bellows are flexible, which can help the fluid move back when the external force is changed or removed. The damping is mainly generated by the condensation effect when the fluid flowing through the hole.

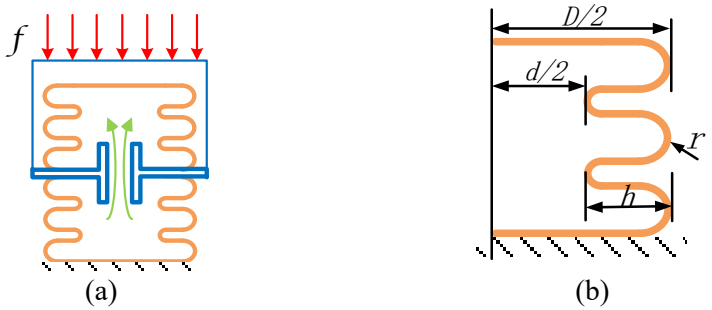


**Figure 6.** (a) is schematic diagram of fluid damping and (b) shows the dimensions of the bellow.

The empirical formula for the axial stiffness of bellows is [14]:

$$K = \frac{\pi}{24n} \frac{D_m E h_0^3 \left(d / D_m\right)^{3/2} C}{\left(D - D_m\right)^3} \tag{26}$$

where $E$ is the Young's modulus. Shown in figure 6 (b), $n$ is the number of layers of the bellows; $r$ is the radius of the fillet; $D_m$ is the average diameter of bellows, $D_m = (D+d)/2$, where $D$ and $d$ are the outer and inner diameter, respectively; $h_0$ is the theoretical thickness of the bellows' wall; $C$ is the shape correction factor, which can be written as:

$$C = \left[ 0.046\left(\frac{r}{H}\right)^3 - 0.144\left(\frac{r}{H}\right)^2 + 0.287\frac{r}{H} + 0.082 \right]^{-1} \tag{27}$$

As shown in figure 7, there is a $3/4$ ring hole on the piston, which the fluid can flow through. Energy dissipation is mainly caused by the contraction before outlet and expanding after outlet.

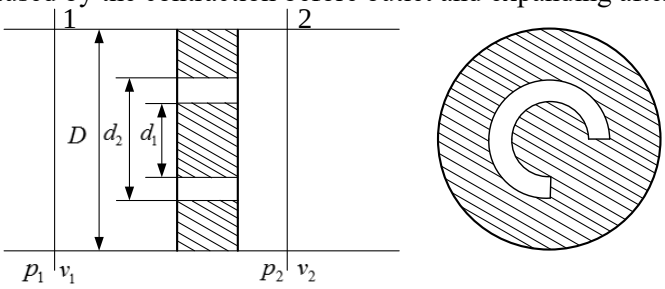


**Figure 7.** Cross Section diagram of damper and piston

$v_1$, $p_1$ are the velocity and pressure at cross section 1; $v_2$, $p_2$ are the velocity and pressure at cross section 2; $v_0$ is the velocity when the fluid flow in the ring hole; the equivalent inner diameter of the cavity is $D$; $d_1$ and $d_2$ are the inner diameter and outer diameter of the ring hole, respectively; the fluid density is $\rho$; the acceleration of gravity is $g$.

According to the law of mass conservation, the Bernoulli equation is given by

$$\frac{p_1}{\rho g} + \frac{\alpha_1 v_2^2}{2g} = \frac{p_2}{\rho g} + \frac{\alpha_2 v_2^2}{2g} + h_w \tag{28}$$

$h_w$ is the loss coefficient due to shrinkage effect:

$$h_w = \zeta \frac{v_0^2}{2g} \tag{29}$$

where $\zeta$ is the resistance loss coefficient.

Assuming $\alpha_1 = \alpha_2 = 1$, and taking the incompressible flow into account, $v_1 = v_2$, the pressure difference between two sides of the ring hole is obtained:

$$\Delta p = p_1 - p_2 = \zeta \frac{\rho v_0^2}{2} \tag{30}$$

According to the continuity of flow,

$$v_1 A = v_0 A_0 \tag{31}$$

where $A = \pi D^2/4$ and $A_0 = 3\pi\left(d_2^2 - d_1^2\right)/16$ are the inner cross section of the cavity and cross section of the ring hole, respectively. The damping force can be defined as:

$$F = \Delta p \cdot A = \frac{\zeta\rho}{2}\frac{A^3}{A_0^2}v^2 \tag{32}$$

Substituting $A$ and $A_0$ into equation (32), one can write:

$$F = \Delta p \cdot A = \frac{2\rho\pi D^6 \zeta}{9\left(d_2^2 - d_1^2\right)^2} v_1^2 = c_h v_1^2 \tag{33}$$

The displacement function of a harmonic motion with frequency $\omega$ and amplitude $X$ is expressed as:

$$x(t) = X \sin(\omega t) \tag{34}$$

The equivalent damping force can be written as:

$$F = c_{eq} v = c_{eq} \omega X \cos(\omega t) \tag{35}$$

where $c_{eq}$ is the equivalent linear damping coefficient. The energy dissipated by the equivalent damping force in one cycle is derived as follows:

$$W = \int_0^{2\pi/\omega} F dx = \int_0^{2\pi/\omega} c_{eq} \left[\omega X \cos(\omega t)\right]^2 dt = c_{eq} \omega \pi X^2 \tag{36}$$

And the energy dissipated by the damping force derived by equation (33) is given as:

$$W = \int_0^{2\pi/\omega} F dx = \int_0^{2\pi/\omega} c_h \left[\left|\omega X \cos(\omega t)\right|\right]^3 dt = \frac{8\omega^2 X^3 c_h}{3} \tag{37}$$

Solving equation (33) and equation (36) , the equivalent linear damping coefficient is obtained

$$c_{eq} = \frac{8\omega X c_h}{3\pi} \tag{38}$$

By looking at equation (38) , the conclusion is that the equivalent linear damping coefficient is not a constant. It is not only related to the structural parameters of the damping holes, but also with the amplitude and frequency of the excitation force.

## 4. Experiments

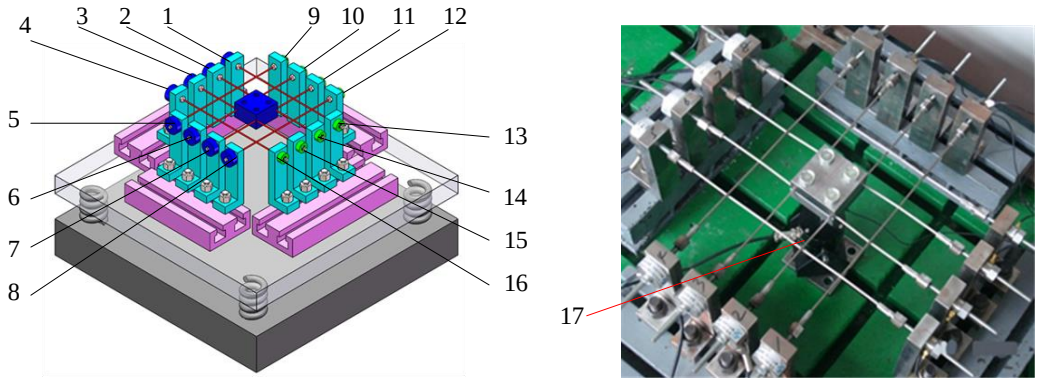


**Figure 8.** Experiment on tension variation of the plane cable net structure.

The tension variation is tested to get the real frequency response of the plane cable net structure, which is used to verify the model set up in this paper. As shown in figure 8, the plane cable net structure is composed of 8 cables, with a mass coupled with the central four intersections. The cables, which are directly connected with the mass, are defined as ‘bearing strings’. The others, which are not directly connected with the cables, are called ‘non-bearing strings’. A static force sensor and a dynamic force sensor are placed on the two ends of cable. The static force sensor is used to demarcate the pretension of the cable and the dynamic force sensor is used to obtain the tension variation in the course of vibration, as shown in table 1. The exciter is mounted on the foundation support, with a random excitation force applied at the centre of the mass. A dynamic force sensor is attached between the exciter and the mass, which is used to measure the force that the exciter transmitted to the mass. Before the experiment, the pretension of the eight cables is adjusted to ensure that they have the same initial preload.

**Table 1.** Sensor parameters and functions.

| | The sensor type | Sensitivity | Utility |
|---|---|---|---|
| 1~8 | Static force sensor | 9.67~9.83 $mV/N$ | Get the initial tension of the table |
| 9~16 | dynamic force sensor | 1000 $mV/N$ | Get the dynamic tension of the table |
| 17 | dynamic force sensor | 100 $mV/N$ | Get the dynamic excitation force of the exciter |

The pretension of the cables is about $300N$, with error less than 2%. The dynamic tension variation of cables at the ends are measured, and the frequency response curves are shown in figure 9. The horizontal coordinate is frequency and the vertical coordinate is the ratio of the dynamic tension variation amplitude and the excitation force amplitude, namely the force transmission characteristic. The dynamic force sensor 15 shows the tension variation of a 'bearing strings' and the dynamic force sensor presents the tension variation of a 'non-bearing strings'. The first order natural frequency is about 21.79 Hz, which is the translation frequency of the mass. The second order to the forth order natural frequency are 62.57 Hz, 119.29 Hz and 179.37 Hz, with multiple relations among them. The amplitude of the tension varying of the 'non-bearing strings' is smaller than the amplitude of the 'bearing strings', which is verified by computation and shown in figure 5.

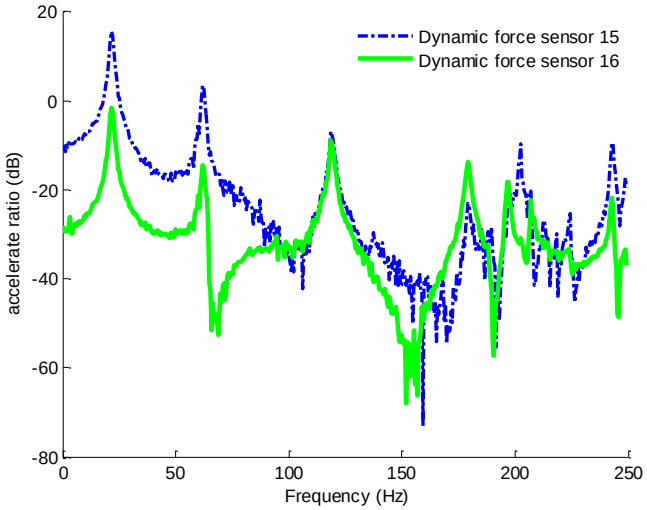


**Figure 9.** Tension variation of the plane cable net structure.

In the experiment, the suspension method is used to simulate the space weightlessness environment. The fluid damper, the plane cable net structure and the isolator composed of the former two are used as the isolation device between the vibration source and the payload. The test procedure is shown in figure 10. The exciter applies a random force on the mass, and the vibration (displacement, velocity and acceleration included) is transmitted to the other mass by the isolator between them. The acceleration data will be obtained by the two acceleration sensor attached to the two masses. The real graph of experimental test is shown is figure 11. The two masses are both 6 $Kg$. The acceleration transmissibility of the isolator is obtained by the ratio of the two accelerations of the two mass, with a random excitation in the range of 0 ~ 250 Hz.

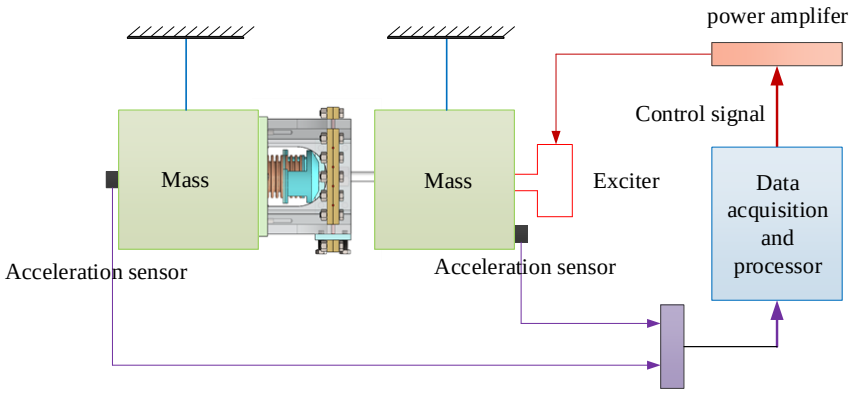


**Figure 10.** The testing procedure.

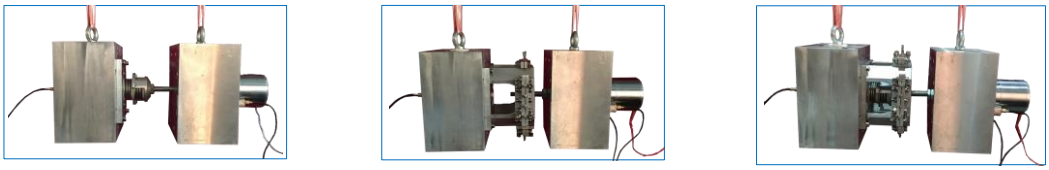

**(a)** (b) (c)

**Figure 11**. Real graph of experimental test: (a) is the fluid damper; (b) is the plane cable net structure and (c) is the isolator composed of the former two in parallel.

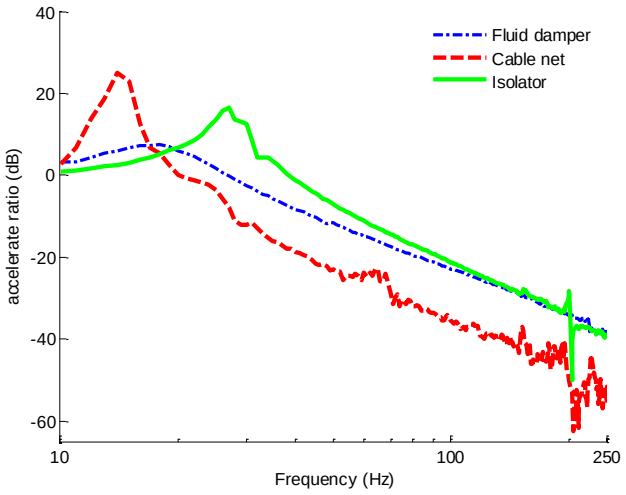


**Figure 12.** The acceleration transmissibility of different isolation device.

As shown in figure 12, results show that the isolation effect of the plane cable net structure is acceptable, and the vibration attenuation rate is about -40 dB/dec in the isolation zone. However, the resonance amplification is high due to the low damping factor of the cables. The fluid damper has a lower resonance amplification, with disadvantages of lower vibration attenuation rate and lower capacity. When the plane cable net structure utilized in parallel with the fluid damper, the resonance peak is significantly decreased and the vibration attenuation rate is close to -38 dB/dec.

## 5. Conclusions

The coupled functions of the transversal and longitudinal vibrations of strings are obtained from the differential equations of motion. According to Hooke's law, the influence of the transversal vibration

and the longitudinal vibration on the string tension is derived. Results show that the latter is much smaller than the former, which is always being ignored in classical string theory.

Based on the mechanical admittance method, a plane cable net structure composed of 8 strings is developed, with tension variation being computed and tested. The vibration of the mass mounted in the centre of the plane cable net structure can be transmitted to the foundations with the strings' tension variation. The displacement response of the mass is very similar to the frequency response of the spring oscillator, with the possibility of being used as a vibration isolator. To avoid the small damping coefficient of the plane cable net structure, a fluid damper made up by bellows is introduced.

Experiments on the plane cable net structure, the fluid damper and the isolator composed by the former two are carried out, respectively. Results show that the isolator has an acceptable resonance amplification and vibration attenuation rate, when compared to the plane cable net structure and the fluid damper.

## 6. References

[1] Aglietti, G., et al. Model building and verification for active control of microvibrations with probabilistic assessment of the effects of uncertainties 2004 *Proceedings of the Institution of Mechanical Engineers, Part C: Journal of Mechanical Engineering Science*. **218**(4): p. 389-399.

[2] Kamesh, D., R. Pandiyan, and A. Ghosal Modeling, design and analysis of low frequency platform for attenuating micro-vibration in spacecraft 2010 *Journal of sound and vibration*. **329**(17): p. 3431-3450.

[3] Zhou, W.-Y. and D.-X. Li Design and analysis of an intelligent vibration isolation platform for reaction/momentum wheel assemblies 2012 *Journal of Sound and Vibration*. **331**(13): p. 2984-3005.

[4] Davis, L.P., D.R. Carter, and T.T. Hyde. *Second-generation hybrid D-strut*. in *Smart Structures & Materials' 95*. 1995. International Society for Optics and Photonics.

[5] Preumont, A., et al. A six-axis single-stage active vibration isolator based on Stewart platform 2007 *Journal of sound and vibration*. **300**(3): p. 644-661.

[6] Davis, L.P., et al. Hubble space telescope reaction wheel assembly vibration isolation system 1986 *NASA Marshall Space Flight Center, Huntsville, Alabama*. **9**.

[7] Vaillon, L. and C. Philippe Passive and active microvibration control for very high pointing accuracy space systems 1999 *Smart materials and structures*. **8**(6): p. 719.

[8] Makihara, K., J. Onoda, and K. Minesugi New approach to semi-active vibration isolation to improve the pointing performance of observation satellites 2006 *Smart materials and structures*. **15**(2): p. 342.

[9] Cobb, R.G., et al. Vibration isolation and suppression system for precision payloads in space 1999 *Smart Materials and Structures*. **8**(6): p. 798.

[10] Sullivan, L.A., et al. On-orbit active vibration isolation: The satellite ultraquiet isolation technologies experiment (SUITE) 2003 *Space*: p. 23-25.

[11] Fusaro, R.L., *Preventing spacecraft failures due to tribological problems*. 2001: Society of Tribologists and Lubrication Engineers.

[12] Bank, B. and L. Sujbert. *A piano model including longitudinal string vibrations*. in *Proceedings of the Digital Audio Effects Conference*. 2004.

[13] Jetmundsen, B., R.L. Bielawa, and W.G. Flannelly Generalized frequency domain substructure synthesis 1988 *Journal of the American Helicopter Society*. **33**(1): p. 55-64.

[14] Minghao, G. Yu miao Rigidity study of cryogenic elastic element for space [J] 2006 *Cryogenics*. **6**.